Inorg. Chem. **2003**, *42*, 6709–6722

Reversible Guest Exchange and Ferrimagnetism (T_C = 60.5 K) in a Porous Cobalt(II)–Hydroxide Layer Structure Pillared with *trans*-1,4-Cyclohexanedicarboxylate

Mohamedally Kurmoo,*,† Hitoshi Kumagai,†,§ Suzanne M. Hughes,‡ and Cameron J. Kepert*,‡

Groupe des Materiaux Inorganiques, Institut de Physique et Chimie des Matériaux de Strasbourg, 23 Rue du Loess, 67037 Strasbourg Cedex, France, and School of Chemistry, University of Sydney, NSW 2006, Australia

Received July 8, 2003

The synthesis, characterization, and reversible guest-exchange chemistry of a new porous magnetic material that orders ferrimagnetically at 60.5 K are described. The material, $Co_5(OH)_8(chdc)\cdot 4H_2O$ (chdc = *trans*-1,4-cyclohexanedicarboxylate), contains tetrahedral–octahedral–tetrahedral Co(II)–hydroxide layers of composition $Co^{(oct)}_3Co^{(tet)}_2(OH)_8$ that are linked together by bis(unidentate) chdc pillars. Noncoordinated water molecules occupy 1-D channels situated between the chdc pillars. The material remains monocrystalline during dehydration from $Co_5(OH)_8(chdc)\cdot 4H_2O$ (CDCC·$4H_2O$) to $Co_5(OH)_8(chdc)$ (CDCC) via an intermediate $Co_5(OH)_8(chdc)\cdot 2H_2O$ (CDCC·$2H_2O$) upon heating or evacuation. In-situ single crystal and powder X-ray diffraction analyses indicate that the interlayer spacing decreases in two steps, each corresponding to the loss of two water molecules per formula unit as determined by thermogravimetry. The single crystal structure of the fully dehydrated material, CDCC, has no void volume due to a tilting of the pillars and 9% decrease of the interlayer spacing with water removal. Exposure of CDCC to air causes rapid rehydration of this material to CDCC·$4H_2O$, as determined by single crystal X-ray diffraction, powder X-ray diffraction, thermogravimetry, and vibrational spectroscopy. Both the hydrated and dehydrated forms order magnetically below 60.5 K. The susceptibility data are consistent with ferrimagnetic behavior, and the value of the saturation magnetization at 2 K (ca. 2 μ_B) is explained by a model of two sublattices, one comprising three octahedral cobalt atoms and another comprising two tetrahedral cobalt atoms. There is an enhanced 2-D correlation within the layer at temperatures just above the Curie temperature, as seen by nonlinearity in the ac susceptibility data and remanence in the isothermal magnetization. The crossover from 2-D to 3-D ordering occurs at T_C. The large anisotropy in the magnetization data on a single crystal suggests either a 2-D Ising or an XY magnet while the critical exponent of 0.25 is in favor of the latter. Both magnetization data in a small field in the ac and dc mode and isothermal magnetization data provide evidence of a further change in behavior at 23 K, which may originate from a reorientation of the moments within the layer. Variation of the pillar and of the guest-exchange chemistry, including the exchange of magnetic guests such as O_2, offers the possibility of tailoring the magnetic properties of this material.

Introduction

Inorganic−organic hybrid materials have received considerable recent attention due to their novel structures and physical/chemical properties. Developments in this broad area have arisen on many fronts and have seen the emergence of properties more commonly associated with nonmolecular solids, such as magnetic ordering,[1] electrical conductivity/superconductivity,[2] and reversible guest exchange/nanoporosity.[3,4] Much of the impetus for this research has been the enormous diversity afforded by hybrid materials, allowing structural arrangements not otherwise accessible in the solid state. The particularly versatile chemistry of these materials has also allowed the strategic coexistence of multiple properties within the one material, with examples including

* Corresponding authors. E-mail: kurmoo@ipcms.u-strasbg.fr (M.K.); kepert_c@chem.usyd.edu.au (C.J.K.).
† Institut de Physique et Chimie des Matériaux de Strasbourg.
‡ University of Sydney.
§ On leave from Applied Molecular Science, Institute for Molecular Science (IMS), Nishigounaka 38, Myoudaiji, Okazaki 444-8585, Japan.

(1) Kahn, O. *Acc Chem. Res.* **2000**, *33*, 647. Day, P. *J. Chem. Soc., Dalton Trans.* **2000**, 3483. Miller, J. S. *Inorg. Chem.* **2000**, *39*, 4392. Gatteschi, D. *Adv. Mater.* **1994**, *6*, 635.

10.1021/ic034787g CCC: $25.00
Published on Web 09/25/2003

magnetic conductors[5] and superconductors,[6] spin-crossover magnets,[7] and nanoporous spin-crossover systems.[8] Here we address the coexistence of magnetism and porosity in the one material.

The generation of open framework materials that order magnetically is an important goal within materials chemistry. Such materials provide a unique mechanism for systematically exploring structure/magnetic-property relationships, since structural perturbation of the magnetic host may be achieved through the exchange of guest species. Further, interesting possibilities exist for the application of such materials in the recognition/separation of molecules according to their magnetic susceptibility (e.g., O_2/N_2). The achievement of high magnetic ordering temperatures in porous materials represents a major challenge. For 3-D magnetic systems, the achievement of short through-space or ligand-mediated exchange interactions in many cases precludes the possibility of achieving significant pore volume.[9−11] The linking together of high magneto-anisotropy systems of lower dimensionality (i.e., 2-D layers, 1-D chains, or 0-D clusters) into robust 3-D lattices provides an important further synthetic approach. Examples of open framework magnetic materials include members of the 3-D cyanide-bridged Prussian blue family, which display reversible dehydration/rehydration[12] and order magnetically above room temperature in some cases;[13] 3-D phosphate-bridged materials,[14,15] hydroxyl-bridged materials,[9] $[Cu_2(Sala)_2(H_2O)]$, for which irreversible dehydration to $[Cu_2(Sala)_2]$ leads to an increase in the ordering temperature for canted antiferromagnetism;[17] and carboxylate-bridged materials.[16,18,19] Further, the (reversible) dehydration of a number of paramagnetic clathrate-type systems has generated polymeric materials that display magnetic ordering.[20]

Within the class of lower-dimensional magnetic systems, the pillaring of inorganic layers having high magneto-anisotropy represents an important strategy for the generation of porous magnets. Notably, a wide range of nonmagnetic pillared-layer materials is well-known to display excellent host−guest properties.[4,9,21−23] Of a number of layered magnetic phases,[11] the metal hydroxides are known for their absorption of guest species via intercalation and, as such, are excellent candidates for a coexistence of porosity and magnetic ordering. Most prominent among these are the layered double hydroxides (LDHs), for which the host−guest chemistries have been investigated extensively.[22,24,25] We have recently reported two pillared-layer compounds, $Co_4(SO_4)(OH)_6(pillar)_{0.5}\cdot xH_2O$ (pillar = 1,2-diaminoethane (en), 4,4-diazabicyclo[2,2,2]octane (dabco); $x = 3$, 1), with the sulfate-containing namuwite-type layer structure that displays reversible dehydration/rehydration, which order as canted

(2) Ishiguro, T.; Yamaji, K.; Saito, G. *Organic Superconductors*, 2nd ed.; Springer-Verlag: New York, 1998. Proceedings of the Symposium on Twenty Years of Organic Superconductors: New Materials, New Insights. Proceedings of the International Chemical Congress of the Pacific Basin Societies; PACIFICHEM, Honolulu, Hawaii, 2000; Geiser, U., Kobayashi, H., Eldridge, J. E., Eds.; *Mol. Cryst. Liq. Cryst.* **2002**, *380*, 1−287. Kepert, C. J.; Kurmoo, M.; Day, P. *Proc. R. Soc. London, Ser. A* **1998**, *454*, 487.

(3) Biradha, K.; Hongo, Y.; Fujita, M. *Angew. Chem., Int. Ed.* **2000**, *39*, 3843. Ferey, G.; Cheetham, A. K. *Science* **1999**, *283*, 1125. Kepert, C. J.; Rosseinsky, M. J. *Chem. Commun.* **1999**, 375. Yaghi, O. M.; Li, G. M.; Li, H. L. *Nature* **1995**, *378*, 703. Hoskins, B. F.; Robson, R. *J. Am. Chem. Soc.* **1990**, *112*, 1546. Kepert, C. J.; Prior, T. J.; Rosseinsky, M. J. *J. Am. Chem. Soc.* **2000**, *122*, 5158.

(4) Kondo, M.; Okubo, T.; Asami, A.; Noro, S.; Yoshitomi, T.; Kitagawa, S.; Ishii, T.; Matsuzaka, H.; Seki, K. *Angew. Chem., Int. Ed.* **1999**, *38*, 140.

(5) Coronado, E.; Galan-Mascaros, J. R.; Gomez-Garcia, C. J.; Laukhin, V. *Nature* **2000**, *408*, 447.

(6) Kurmoo, M.; Graham, A. W.; Day, P.; Coles, S. J.; Hursthouse, M. B.; Caulfield, J. L.; Singleton, J.; Pratt, F. L.; Hayes, W.; Ducasse, L.; Guionneau, P. *J. Am. Chem. Soc.* **1995**, *117*, 12209.

(7) Brooker, S.; Plieger, P. G.; Moubaraki, B.; Murray, K. S. *Angew. Chem., Int. Ed.* **1999**, *38*, 408. Sieber, R.; Decurtins, S.; Stoeckli-Evans, H.; Wilson, C.; Yufit, D.; Howard, J. A. K.; Capelli, S. C.; Hauser, A. *Chem. Eur. J.* **2000**, *6*, 361.

(8) Halder, G. J.; Kepert, C. J.; Moubaraki, B.; Murray, K. S.; Cashion, J. D. *Science* **2000**, *298*, 1762.

(9) Barthelet, K.; Marrot, J.; Riou, D.; Ferey, G. *Angew. Chem., Int. Ed.* **2001**, *41*, 281.

(10) Metal-Organic and Organic Molecular Magnets. Discussion Meeting March, 24−25, 1999; Day, P., Underhill, A. E., Eds.; *Philos. Trans. R. Soc. London, Ser. A* **1999**, *357*, 1−333. Magnetism: A Supramolecular Function. Proceedings of the NATO Advanced Research Workshop on Magnetism: A Supramolecular Function; Carcans-Maubuisson, France, September 16−20, 1995; Kahn, O., Ed.; *NATO ASI Ser., Ser. C* **1996**, *484*. *Molecular Magnetism, New Magnetic Materials*; Itoh, K., Kinoshita, M., Eds.; Gordon Breach-Kodansha: Tokyo, 2000.

(11) *Magnetic Properties of Layered Transition Metal Compounds*; de Jongh, L. J.; Ed.; Kluwer Academic Publishers: Dordrecht, 1990.

(12) Buser, H. J.; Gideon, R.; Ludi, A.; Engel, P. *J. Chem. Soc., Dalton Trans.* **1974**, *23*, 2473. Beauvais, L. G.; Long, J. R. *J. Am. Chem. Soc.* **2002**, *124*, 12096.

(13) Verdaguer, M.; Bleuzen, A.; Marvaud, V.; Vaissermann, J.; Seuleiman, M.; Desplanches, C.; Scuiller, A.; Train, C.; Garde, R.; Gelly, G.; Lomenech, C.; Rosenman, I.; Veillet, P.; Cartier, C.; Villain, F. *Coord. Chem. Rev.* **1999**, *190−192*, 1023. Mallah, T.; Thiebaut, S.; Verdaguer, M.; Veillet, P. *Science* **1993**, *262*, 1554. Ferlay, S.; Mallah, T.; Ouahes, R.; Veillet, P.; Verdaguer, M. *Nature* **1995**, *378*, 701.

(14) Cavellec, M.; Riou, D.; Greneche, J. M.; Ferey, G. *J. Magn. Magn. Mater.* **1996**, *163*, 173. Cavellec, M.; Riou, D.; Ninclaus, C.; Greneche, J. M.; Ferey, G. *Zeolites* **1996**, *17*, 250.

(15) Riou-Cavellec, M.; Greneche, J. M.; Ferey, G. *J. Solid State Chem.* **1999**, *148*, 150.

(16) Livage, C.; Egger, C.; Ferey, G. *Chem. Mater.* **1999**, *11*, 1546.

(17) Yang, X. D.; Si, L.; Ding, J.; Ranford, J. D.; Vittal, J. J. *Appl. Phys. Lett.* **2001**, *78*, 3502. Ranford, J. D.; Vittal, J. J.; Wu, D. Q.; Yang, X. D. *Angew. Chem., Int. Ed.* **1999**, *38*, 3498.

(18) Riou-Cavellec, M.; Albinet, C.; Livage, C.; Guillou, N.; Nogues, A.; Greneche, J. M.; Ferey, G. *Solid State Sci.* **2002**, *4*, 267.

(19) Zhang, X. X.; Chui, S. S. Y.; Williams, I. D. *J. Appl. Phys.* **2000**, *87*, 6007.

(20) Kahn, O.; Larionova, J.; Yakhmi, J. V. *Chem. Eur. J.* **1999**, *5*, 3443. Chavan, S. A.; Larionova, J.; Kahn, O.; Yakhmi, J. V. *Philos. Mag. B* **1998**, *77*, 1657. Larionova, J.; Chavan, S. A.; Yakhmi, J. V.; Froystein, A. G.; Sletten, J.; Sourisseau, C.; Kahn, O. *Inorg. Chem.* **1997**, *36*, 6374. Nakatani, K.; Bergerat, P.; Codjovi, E.; Mathoniere, C.; Yu, P.; Kahn, O. *Inorg. Chem.* **1991**, *30*, 3977.

(21) Evans, O. R.; Lin, W. B. *Inorg. Chem.* **2000**, *39*, 2189. O'Hare, D. *New J. Chem.* **1994**, *18*, 989. Forster, P. M.; Cheetham, A. K. *Angew. Chem., Int. Ed.* **2002**, *41*, 457. Figueras, F. *Catal. Rev.−Sci. Eng.* **1988**, *30*, 457. Gomez-Lor, B.; Gutierrez-Puebla, E.; Iglesias, M.; Monge, M. A.; Ruiz-Valero, C.; Snejko, N. *Inorg. Chem.* **2002**, *41*, 2429; Burch, R. *Catal. Today* **1988**, *2*, 185. Jacobson, A. J. In *Solid State Chemistry: Compounds*; Oxford University Press: Oxford, 1992; pp 182. Pinnavaia, T. J. *Science* **1983**, *220*, 365. Schoellhorn, R. *Inclusion Compd.* **1984**, *1*, 249. Clearfield, A. *Curr. Opin. Solid State Mater. Sci.* **1996**, *1*, 268. Clearfield, A. *Chem. Rev.* **1988**, *88*, 125. Clearfield, A. In *Progress in Inorganic Chemistry*; Karlin, K. D., Ed.; Wiley: New York, 1998; Vol. 47, p 371. Cao, G.; Hong, H.; Mallouk, T. E. *Acc. Chem. Res.* **1992**, *25*, 420. Gavin, J. A. *Acc. Chem. Res.* **1998**, *31*, 209. O'Hare, D. In *Inorganic Materials*; Bruce, D. W., O'Hare, D., Eds.; Wiley: London, 1993.

(22) Newman, S. P.; Jones, W. *New J. Chem.* **1998**, *22*, 105. Ohtsuka, K. *Chem. Mater.* **1997**, *9*, 2039.

(23) Kitaura, R.; Fujimoto, K.; Noro, S.; Kondo, M.; Kitagawa, S. *Angew. Chem., Int. Ed.* **2002**, *41*, 133.

(24) Newman, S. P.; Jones, W. *J. Solid State Chem.* **1999**, *148*, 26.

(25) Wang, J. D.; Serrette, G.; Tian, Y.; Clearfield, A. *Appl. Clay Sci.* **1995**, *10*, 103.

antiferromagnets below 21 K and display metamagnetic behavior with critical fields of up to 2 kOe.[26] In these materials, the structural robustness to guest dehydration/rehydration was seen to depend on the rigidity of the organic pillar, the layers of the en-pillared phase collapsing with dehydration whereas the dabco-pillared phase displays 3-D robustness.

For the divalent transition metal hydroxides, we[27] and others[24] have recently shown that, depending on the transition metal, one of two basic structures arise: copper(II) and nickel(II) form single CdI_2-type metal−hydroxide layers, while cobalt(II) and zinc(II) form a number of different triple-decker layers containing both octahedral and tetrahedral metal ions. In these materials, the rigid metal−hydroxide layers have been interleaved with a range of moieties that include alkyl- or aryl-carboxylates, dicarboxylates, sulfonates, and organonitriles.[27] For the magnetic analogues, a lack of highly crystalline samples has hampered characterizations of their structures and magnetic properties:[27−30] in particular, the different ground states for the various layered materials have yet to be correlated with structure type, and the nature of the magnetic dimensionality with regard to the long-range magnetic ordering remains to be understood. For many of the cobalt compounds, it has been inferred from powder X-ray and electron diffraction that the layer structure is similar to that of $[Zn_5(OH)_8(H_2O)_2](NO_3)_2$,[24,27,31] which contains layers of octahedrally coordinated zinc(II) where one in four is periodically removed and each vacant hole is sandwiched by two tetrahedrally coordinated zinc(II) ions. We have previously proposed that dicarboxylate ligands may bridge such layers into stable three-dimensional structures.[27] In persistent attempts to produce single crystals of such materials for full structure determination, we have adopted two strategies: first, the recrystallization of powders using the hydrothermal technique, and, second, the use of a wide range of innocent co-solute molecules to control pH and assist in the initiation of crystal growth. Here, we report the successful synthesis of single crystals of $Co_5(OH)_8(chdc)\cdot 4H_2O$ (chdc = *trans*-1,4-cyclohexanedicarboxylate) formed in the presence of barbituric acid as a co-solute. The material orders ferrimagnetically at 60.5 K and displays reversible dehydration/rehydration. Magnetic measurements of the hydrated and dehydrated forms indicate that the magnetic properties are insensitive to the degree of hydration and that the system is XY with a crossover from 2-D to 3-D occurring at the Curie temperature. Measurements on an aligned single crystal indicate that the magnetic easy axis lies in the plane of the layer and not perpendicular to it. The easy axis perpendicular to the layer was inferred previously for related materials from the observation of the large coercive fields.[27−29]

Experimental Section

Synthesis. All chemicals were obtained from Aldrich and Fluka and used without further purification. A solution of $Co(NO_3)_2\cdot 6H_2O$ (2 mmol) was added to a neutral solution of a mixture of *cis*- and *trans*-1,4-cyclohexanedicarboxylic acid (1 mmol) and NaOH (2 mmol) followed by addition of barbituric acid (2 mmol). An aqueous solution of NaOH (2 mmol) was added to give an amorphous blue precipitate. The mixture was placed in a Teflon lined hydrothermal autoclave, which was sealed and placed in an oven at 170 °C for 16 h. The bomb was cooled in a water bath, and the barbituric acid was separated from the crystals of CDCC·$4H_2O$ by flotation in a water/ethanol mixture and decantation. The deep blue rectangular platelet crystals were washed with acetone and dried in air. % Calcd (Found) for $C_8H_{26}Co_5O_{16}$: C 14.28 (14.28), H 3.89 (3.72), Co 43.79 (43.7). Infrared bands (cm^{-1}) of a virgin sample: 619w, 630w, 778mbr, 923w, 1011w, 1212m, 1280m, 1330w, 1362w, 1392s, 1450w, 1542vs, 1618wsh, 2858m, 2926msh, 2942m, 3372sbr, 3446sbr, 3516mbr, 3580m sharp.

X-ray Crystallography and Structure Solution. Single crystal data were collected on a Bruker AXS SMART 1000 CCD diffractometer equipped with graphite-monochromated Mo Kα radiation ($\lambda = 0.7017$ Å) and an Oxford Nitrogen Cryostream. A thin rectangular platelet of CDCC·$4H_2O$ of dimensions $0.27 \times 0.09 \times 0.01$ mm^3 was mounted inside an open-ended 0.3 mm glass capillary with a thin smear of grease. This crystal was used for five separate full crystallographic data collections. The crystal was first quench-cooled to −123(2) °C, and a full data set was collected. The same crystal was later warmed in the dinitrogen cryostream at a rate of 20 °C/h from room temperature to 102(2) °C during which diffraction images were collected to monitor unit cell changes as the crystal was dehydrated from CDCC·$4H_2O$ to CDCC. Full data sets were collected at 102(2) and −123(2) °C on this phase. The crystal was removed from the dinitrogen stream and left to stand in air ($T = 22(2)$ °C, relative humidity = 35(5)%) for two weeks to allow gradual rehydration to CDCC·$4H_2O$, after which full data collections were made at 22(2) °C in air and at −123(2) °C under dinitrogen.

Diffraction data analysis and reduction were performed within SMART and SAINTPLUS.[32] The data sets of the fully desolvated crystal, CDCC, showed slight twinning, with the minor twin having intensities ca. $^1/_{10}$ those of the major twin. Indexing for the principal twin component was achieved using GEMINI,[33] and integration of the severely broadened, overlapping diffraction spots was achieved by manual variation of the box size to optimize the merging and crystal refinement indices. Systematic errors in the spot integration restrict the quality of these data sets. The twinning disappeared on rehydration to CDCC·$4H_2O$, and the spot widths decreased substantially. Diffraction images of the crystal in its virgin, dehydrated, and rehydrated forms are given in Figure S1 of the Supplementary Information. The data sets for both virgin and rehydrated CDCC·$4H_2O$ were corrected for absorption by face-

(26) Rujiwatra, A.; Kepert, C. J.; Rosseinsky, M. J. *Chem. Commun.* **1999**, 2307. Rujiwatra, A.; Kepert, C. J.; Claridge, J. B.; Rosseinsky, M. J.; Kumagai, H.; Kurmoo, M. *J. Am. Chem. Soc.* **2001**, *123*, 10584.
(27) Kurmoo, M.; Day, P.; Derory, A.; Estournes, C.; Poinsot, R.; Stead, M. J.; Kepert, C. J. *J. Solid State Chem.* **1999**, *145*, 452. Kurmoo, M. *Mol. Cryst. Liq. Cryst.* **2000**, *341*, 1199. Kurmoo, M. *Chem. Mater.* **1999**, *11*, 3370. Kurmoo, M. *Mol. Cryst. Liq. Cryst.* **2000**, *342*, 167. Jestädt, T.; Kurmoo, M.; Blundell, S. J.; Lovett, B. W.; Pratt, F. L.; Hayes, W. *Synth. Met.* **1999**, *103*, 2325. Kurmoo, M. *J. Mater. Chem.* **1999**, *9*, 2595.
(28) Kurmoo, M. *Philos. Trans. R. Soc. London, Ser. A* **1999**, *357*, 3041.
(29) Kurmoo, M.; Kumagai, H. *Mol. Cryst. Liq. Cryst.* **2002**, *376*, 555. Kurmoo, M.; Kumagai, H.; Green, M. A.; Lovett, B. W.; Blundell, S. J.; Ardavan, A.; Singleton, J. *J. Solid State Chem.* **2001**, *159*, 343. Lovett, B. W.; Blundell, S. J.; Kumagai, H.; Kurmoo, M. *Synth. Met.* **2001**, *121*, 1814.
(30) Kumagai, H.; Akita-Tanaka, M.; Inoue, K.; Kurmoo, M. *J. Mater. Chem.* **2001**, *11*, 2146.
(31) Stählin, W.; Oswald, H. R. *Acta Crystallogr., Sect. B* **1970**, *26*, 860.
(32) *SMART, SAINT and XPREP. Area detector control and data integration and reduction software*; Bruker: Madison, WI, 1995.
(33) *GEMINI Twinning Solution Program Suite*; Bruker: Madison, WI, 1999.

indexed analytical absorption correction followed by empirical absorption correction within SADABS[34] to correct for the grease and glass capillary. For the twinned data sets of CDCC, it was found that analytical absorption correction led to higher refinement indices, and so, only empirical absorption corrections were applied.

The structures were solved and refined using a combination of direct and Fourier methods within SHELXS-86[35] and SHELXL-97.[36] For CDCC·$4H_2O$, the systematic absences indicated two possible space groups, *Imma* and *Ima*2. Structure solution and refinement in *Imma* gave a model with 50% disordered $Co_5(OH)_8$ layers, the two orientations being related by C_2 symmetry along the *b*-axis. Refinement in *Ima*2, a polar subgroup of *Imma*, gave similar refinement indices and a Flack parameter of 0.47(11). Constrained refinement in *P*1 gave disordered layers with 49(1): 51(1) occupation, indicating that the layer disorder is intrinsic to the structure and that *Imma* is the most appropriate space group. Only the nondisordered non-hydrogen atoms, which comprise the cobalt atoms, the atoms of the chdc carboxylate group, and the water oxygen atom, were refined anisotropically. The hydrogen atoms of the water molecule, one of which is disordered over two sites, were located in the electron density map; the bond lengths and angles were constrained so that the O−H distances were equal in each of the disordered orientations. All other hydrogen atoms were located using the riding model. An ORTEP diagram for CDCC·$4H_2O$ is given in Figure S2.

Structural refinement of the dehydrated phase, CDCC, which is more highly disordered than the parent hydrated structure and gave lower quality diffraction data, required the use of several geometric restraints and constraints for stable refinement. All atoms were refined isotropically except Co2 and Co3, which were refined anisotropically but restrained to approximate isotropic behavior. The difference maps contained large, positive peaks lying approximately 1 Å from the cobalt atoms along the *b*-direction, a feature that is symptomatic of systematic errors in the diffraction data caused by the spot streaking along *b**. The carboxylate group of the chdc pillar was well defined in the electron difference map as having two separate orientations with 50% occupation. For the cyclohexane ring of the pillar, only a diffuse electron difference density was observed, indicating severe disorder in this region. Attempts to model a suspected 4-fold disorder of this unit led to unreasonably high correlation between refinement variables. The final structural model incorporates two independent orientations of the chdc pillar, with bond lengths and next-nearest-neighbor distances restrained to values derived from structures within the Cambridge Crystallographic Database[37] and with isotropic thermal parameters of structurally similar atoms fixed to be equal. An ORTEP diagram for CDCC is given in Figure S3.

Powder X-ray Diffractometry (PXRD). The purity and crystallinity of the bulk samples were checked by PXRD using a Siemens D-500 diffractometer equipped with Co Kα radiation ($\lambda = 1.789$ Å) and a secondary quartz monochromator employing the Bragg−Brentano geometry. Temperature- and pressure-dependent diffraction data were collected on an INEL diffractometer equipped with quartz monochromated Co Kα radiation and a curved multidetector.

Thermal Analysis. Thermogravimetric-differential thermal analyses (TG-DTA) were performed in air on a SETARAM system at heating rates of 5 °C/min (20−800 °C) and 0.5 °C/min (20−400 °C) to probe the temperature- and time-dependent dehydration. Cyclic dehydration/rehydration measurements were also performed, in which samples were partially dehydrated by heating at a rate of 30 °C/h to 90 °C, and fully dehydrated by heating to 150 °C to give the anhydrous phase CDCC, before cooling in air to 20 °C to monitor water uptake.

Scanning electron microscopy and electron diffraction measurements were performed both to check the purity of the samples by analysis of their crystallite morphologies and diffraction patterns and to investigate the influence of dehydration, both thermal and in vacuo, on crystal quality. Measurements were performed by transmission on a TOPCON 002B instrument operating at 200 kV. The samples were prepared by allowing a drop of an ethanol suspension of CDCC·$4H_2O$ to dry over a copper grid predeposited with a polymer film. Electron photography was performed on a JEOL JSM-6700F microscope. The high vacuum (10^{-7} Torr) aspect of these techniques causes dehydration of the sample to CDCC.

Vibrational Spectroscopy. FTIR data were collected on a Mattson spectrometer in the mid-IR region (400−4000 cm^{-1}) with a 2 cm^{-1} spectral resolution. The sample films were prepared by dispersing fine particles onto a KBr crystal, thereby avoiding water absorption as commonly encountered with pressed KBr pellets. Temperature-dependent measurements were made using a temperature controlled EUROLABO oven equipped with a platinum thermocouple.

UV−Vis Spectroscopy. UV−vis spectra were recorded by transmission on a Hitachi U-3000 spectrometer. Samples were prepared by setting an array of crystals in poly-methyl methacrylate (PMMA), the transparency of which results in a low background and nearly wavelength-independent baseline by the elimination of scattering encountered on powdered samples.

Magnetic Measurements. Alternating current (ac) and direct current (dc) magnetic measurements were made on a Quantum Design MPMS-XL SQUID magnetometer in the temperature range 2−400 K and with applied fields up to 50 kOe. Alternating current measurements were performed with cooling of the sample in a field of 1 Oe oscillating at 20 Hz. Samples were fixed in gelatin capsules and held in drinking straws. Several temperature and field protocols were employed, as described in the Results section. Isothermal magnetization measurements on aligned crystals were made on samples prepared by suspending the crystals in a solution of PMMA in CH_2Cl_2 and allowing the solvent to evaporate to dryness. This technique leaves the crystals fixed in a specified alignment within the solid polymer and prevents any torque on the crystallites in a magnetic field. The flat platelet crystals were aligned parallel to the surface of the polymer film, allowing measurement both parallel and perpendicular to the *b*-axis (the direction perpendicular to the layers). Measurements were also performed on one single crystal placed on a nonmagnetic silicon chip from Hitachi. The crystal edges were set parallel to the edges of the precisely cut square chip with orientation defined by its crystallographic indexation. The isothermal magnetization of powder samples was measured at different temperatures on a Princeton Applied Research vibrating sample magnetometer model 155 operating at 110 kHz with applied fields of up to 18 kOe. Variable temperatures (4−300 K) were achieved in a continuous flow cryostat with an Oxford Instruments ITC4 temperature controller. Samples were fixed in Perspex containers to prevent motion of the powder on ramping of the field.

Results

Synthesis. The formation of the $Co^{(oct)}_3Co^{(tet)}_2(OH)_8$ layer is highly sensitive to pH and temperature and is favored in

(34) Blessings, R. *Acta Crystallogr., Sect. A* **1995**, *51*, 33.
(35) Sheldrick, G. M. *SHELX86 Programs for Crystal Structure Analysis*; University of Göttingen: Göttingen, Germany, 1986.
(36) Sheldrick, G. M. *SHELX97 Programs for Crystal Structure Analysis*; University of Göttingen: Göttingen, Germany, 1998.
(37) Allen, F. H. *Acta Crystallogr., Sect. B* **2002**, *58*, 380.

Table 1. Summary of Crystal Data and Refinement Results for CDCC·4H_2O at −123(2) °C, CDCC at 102(2) and −123(2) °C, and Rehydrated CDCC·4H_2O at 22(2) and −123(2) °C

compd	CDCC·4(H_2O)	CDCC	CDCC	rehydrated CDCC·4(H_2O)	rehydrated CDCC·4(H_2O)
formula	$Co_5(OH)_8(C_8H_{10}O_4)\cdot 4(H_2O)$	$Co_5(OH)_8(C_8H_{10}O_4)$	$Co_5(OH)_8(C_8H_{10}O_4)$	$Co_5(OH)_8(C_8H_{10}O_4)\cdot 4(H_2O)$	$Co_5(OH)_8(C_8H_{10}O_4)\cdot 4(H_2O)$
fw/g mol^{-1}	672.9(2)	600.87(2)	600.87(2)	672.9(2)	672.9(2)
T/°C	−123(2)	102(2)	−123(2)	22(2)	−123(2)
cryst syst	orthorhombic	triclinic	triclinic	orthorhombic	orthorhombic
space group	*Imma* (No. 74)	$P\bar{1}$ (No. 2)	$P\bar{1}$ (No. 2)	*Imma* (No. 74)	*Imma* (No. 74)
a/Å	12.456(3)	6.213(4)	6.178(10)	12.446(3)	12.484(7)
B /Å	29.027(7)	13.559(8)	13.64(2)	28.860(2)	28.860(2)
c/Å	5.3996(13)	5.437(3)	5.431(9)	5.372(6)	5.372(6)
α/deg	90	85.460(11)	84.89(3)	90	90
β/deg	90	89.954(9)	89.89(3)	90	90
γ/deg	90	82.686(11)	83.84(3)	90	90
V/Å^3	1952.3(8)	452.9(5)	453.0(13)	1944.6(9)	1920.3(11)
Z	4	1	1	4	4
ρ_{calcd} /Mg m^{-3}	2.289	2.203	2.202	2.299	2.328
μ/mm^{-1}	4.237	4.536	4.534	4.254	4.307
data/restraints/params	1240/5/83	1977/42/99	1934/41/72	1210/5/83	1216/5/83
$R(F)$/% {$I > 2\sigma(I)$, all data}	0.0599 {0.0794}	0.1503 {0.1782}	0.1887 {0.2138}	0.0785 {0.1215}	0.0934 {0.1156}
$R_w(F^2)$/% {$I > 2\sigma(I)$, all data}	0.1820 {0.2018}	0.3498 {0.3709}	0.4298 {0.4526}	0.2181 {0.2546}	0.2532 {0.2746}
GOF	1.236	1.198	1.159	1.075	1.209

highly alkaline conditions in the temperature range 170−200 °C. At lower pH and temperatures between 120 and 150 °C, a bridged chain compound consisting of $Co^{(oct)}_3(OH)_2$ is formed predominantly. The layered compound is formed selectively with *trans*-chdc, and the chain compound with *cis*-chdc. The addition of barbituric acid as a co-solute was found not to be essential to the formation of CDCC·4H_2O, although we achieved the highest quality single crystals with its use. The use of other co-solutes such as urea, uracil, and orotic acid did not improve the quality of the crystals. Under these conditions, the hydrothermal syntheses had approximately quantitative yields and gave a high purity product: powder X-ray diffraction patterns of the samples could be fully indexed as CDCC·4H_2O, indicating an absence of any crystalline impurities, and for all of several samples studied by scanning electron microscopy, only an elongated plate morphology of the deep blue crystals was observed, indicating the absence of any amorphous impurities.

3-D Pillared Structure of CDCC·4H_2O. A summary of the crystal data collection and refinement results is given in Table 1. The material consists of cobalt(II) hydroxide layers that are linked by coordinated *trans*-1,4-cyclohexanedicarboxylate pillars (Figure 1). The layers are related to the CdI_2 structure but have one in four of the octahedral Co^{II} sites removed and replaced by two tetrahedral Co^{II} atoms projecting above and below the layer. The tetrahedral coordination about these sites is completed by the unidentate carboxylate groups of the chdc pillars. This tetrahedral−octahedral−tetrahedral layer structure has been seen previously in $[Zn^{II}_5(OH)_8(H_2O)_2](NO_3)_2$,[24,28,31] in which a water molecule completes the tetrahedral metal ion coordination and unbound nitrate anions are located between the layers. Comparisons of the Co−O bond lengths and angles with $Zn_5(OH)_8(H_2O)_2.(NO_3)_2$[31] are given in Tables 2 and 3. The mean tetrahedral and octahedral Co−O distances for CDCC·4H_2O (−123 °C) are 1.98(6) and 2.11(2) Å, which are comparable with those for $Zn_5(OH)_8(H_2O)_2.(NO_3)_2$ of 1.95 and 2.16 Å, respectively.

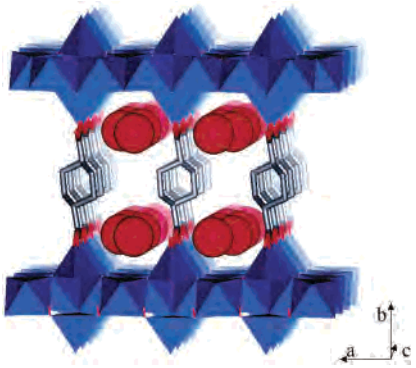

Figure 1. Polyhedral representation of the crystal structure of CDCC·4H_2O, which consists of layers of composition $Co^{(oct)}_3Co^{(tet)}_2(OH)_8$ linked by *trans*-1,4-cyclohexanedicarboxylate pillars that are coordinated to the tetrahedral Co atoms. Water molecules, represented as spheres, occupy 1-D interlayer channels that lie parallel to the *c*-axis. Hydrogen atoms, and the 50% layer and cyclohexane disorder, are omitted for clarity.

The pillared-layer 3-D framework of CDCC·4H_2O houses 1-D interlayer channels that are filled with water of crystallization. The dimensions of the channels, calculated by subtracting off van der Waals radii for the framework atoms, are 3.7 × 2.3 Å^2 in the neighborhood of the water molecule and 3.3 × 2.2 Å^2 at the narrowest point. The channels occupy 13.4% of the crystal volume, corresponding to 262 Å^3 in a unit cell volume of 1952.3 Å^3.[38] Each water molecule occupies a pore volume of 16 Å^3 (cf. packing density of 19 Å^3 per water molecule in ice), indicating that the water molecules are packed highly efficiently within the 1-D channels.

The chdc pillars are oriented to give an exact *c*/2 translation of neighboring $Co_5(OH)_8$ layers within an orthorhombic unit cell, the layers being equivalent and related by body-centering. The layers are randomly disordered between two orientations (A and B), for which the cobalt atom but not the hydroxyl group positions superimpose. Each orienta-

(38) Spek, A. L. *PLATON for Windows*; Utrecht University: Utrecht, The Netherlands, 2000.

Table 2. Metal−Oxygen Bond Lengths for Tetrahedral and Octahedral Cobalt Atoms in CDCC·4H_2O and CDCC and Comparison with the Structural Analogue $Zn_5(OH)_8(NO_3)_2·2H_2O$[31]

	CDCC·4(H_2O)			$Zn_5(OH)_8(NO_3)_2·2H_2O$[31]		CDCC	
	virgin (−123 °C)	rehydrated (22°C)	rehydrated (−123°C)	(22°C)		(102 °C)	(−123 °C)
			Tetrahedral				
Co3−O11	2.019(8)	2.018(10)	2.016(10)	1.963(11)	Co3−O11A	1.90(4)	1.87(3)
					Co3−O11B	1.82(3)	1.82(3)
Co3−O1A	1.995(14)	1.993(19)	1.992(19)	1.937(12)	Co3−O1A	1.96(3)	1.96(4)
Co3−O1B	2.008(13)	2.002(17)	1.988(18)		Co3−O1B	1.91(3)	1.96(4)
Co3−O2A	1.930(9)	1.935(12)	1.943(12)	1.937(12)	Co3−O3A	1.91(3)	1.94(4)
Co3−O2B	1.951(9)	1.951(13)	1.936(11)		Co3−O3B	1.95(4)	1.92(4)
					Co3−O4A	2.00(2)	2.07(4)
					Co3−O4B	2.08(3)	2.05(4)
			Octahedral				
Co1−O1A	2.148(10)	2.157(14)	2.138(13)	2.193(12)	Co1−O1A	2.06(3)	2.11(4)
Co1−O1B	2.055(9)	2.071(12)	2.066(12)	2.193(12)	Co1−O1B	2.16(4)	1.98(3)
Co1−O2A	2.179(9)	2.163(12)	2.154(12)	2.193(12)	Co1−O2A	2.10(2)	2.13(4)
Co1−O2B	2.117(9)	2.113(13)	2.105(12)	2.193(12)	Co1−O2B	2.10(3)	2.09(4)
					Co1−O3A	2.18(3)	2.14(4)
Co1−O3	2.075(10)	2.065(13)	2.077(12)	2.020(11)	Co1−O3B	2.05(4)	2.11(4)
					Co2−O1A	2.10(3)	2.05(4)
					Co2−O1B	2.11(4)	2.11(4)
Co2−O2A	2.161(9)	2.138(12)	2.131(12)	2.160(12)	Co2−O2A	2.11(2)	2.10(4)
Co2−O2B	2.116(9)	2.119(12)	2.099(11)	2.118(11)	Co2−O2B	2.13(3)	2.10(4)
					Co2−O4A	2.16(2)	2.09(4)
Co2−O3	2.063(10)	2.063(11)	2.050(12)	2.089(11)	Co2−O4B	2.11(3)	2.07(3)

Table 3. Bond Angles for Tetrahedral and Octahedral Cobalt Atoms in CDCC·4H_2O and CDCC

	CDCC·4(H_2O)			$Zn_5(OH)_8(NO_3)_2·2H_2O$[31]		CDCC	
	virgin (−123 °C)	rehydrated (22°C)	rehydrated (−123°C)	(RT)		(102 °C)	(−123 °C)
			Tetrahedral				
O11−Co3−O1A	103.6(4)	103.3(6)	103.2(6)	108.5(6)	O11A-Co3−O1B	118.1(16)	121.7(18)
O11−Co3−O1B	106.8(4)	105.2(6)	105.7(4)	115.8(6)	O11B−Co3−O1A	111.3(15)	109.1(18)
O11−Co3−O2A	103.1(3)	103.8(4)	103.4(4)	108.5(6)	O11A-Co3−O3A	115.4(15)	111.7(14)
O11−Co3−O2B	106.4(3)	106.4(4)	106.7(4)	115.8(6)	O11B−Co3−O3B	111.5(17)	104.4(16)
					O11A-Co3−O4A	100.6(14)	105.2(14)
					O11A-Co3−O4B	102.1(15)	100.5(14)
					O11B−Co3−O4A	101.0(15)	100.2(15)
					O11B−Co3−O4B	102.7(16)	105.9(15)
					O1A-Co3−O3A	113.0(12)	111.5(15)
					O1A-Co3−O4A	113.4(10)	116.0(15)
					O3A-Co3−4A	116.5(11)	115.3(15)
					O1B−Co3−3B	111.1(16)	114.2(11)
					O1B−Co3−O4B	115.8(14)	110.2(14)
					O3B−Co3−O4B	112.2(14)	114.4(15)
			Octahedral				
O3−Co1−O1A	96.0(4)	96.0(5)	95.7(5)	83.4(5)	O1A-Co1−O2A	96.4(10)	96.3(14)
O3−Co1−O1B	97.2(4)	96.6(5)	96.9(5)	83.4(5)	O1B−Co1−O2B	94.4(12)	96.4(14)
O3−Co1−O2A	91.7(4)	92.0(4)	91.5(5)	83.4(5)	O1B−Co1−O3B	91.9(14)	92.0(13)
O3−Co1−O2B	94.4(4)	94.4(5)	94.9(5)	83.4(5)	O2B−Co1−O3B	98.2(13)	93.7(14)
					O1A-Co1−O3A	90.5(10	91.8(13)
					O2A-Co1−O3A	93.2(10)	94.8(13)
O1A-Co1−O2A	88.8(4)	89.1(6)	89.0(6)	89.9(5)	O1A-Co2−O2A	95.1(10)	93.2(14)
O1A-Co1−O2B	93.0(5)	93.3(7)	92.9(6)	89.9(5)	O1A-Co2−O4A	91.4(10)	93.1(14)
O1B−Co1−O2A	92.2(5)	92.8(6)	93.3(6)	89.9(5)	O1B−Co2−O2B	94.6(12)	96.4(14)
O1B−Co1−O2B	91.9(4)	90.9(6)	91.3(6)	89.9(5)	O1B−Co2−O4B	93.7(13)	93.2(14)
O3−Co2−O2A	95.6(4)	96.3(5)	95.7(5)	82.6(5)	O2B−Co2−O4B	96.4(12)	94.3(14)
O3−Co2−O2B	95.2(4)	95.3(5)	95.7(5)	96.1(5)	O2A-Co2−O4A	94.0(9)	94.2(14)
O2A-Co3−O2B	91.8(3)	91.5(4)	91.8(5)	89.2(5)			

tion has short hydrogen bonded contacts through the hydroxyl groups to the uncoordinated oxygen atoms of the pillar carboxylate group (O(12)···O(1A) = 2.797(17); O(12)···O(1B) = 2.707(16) Å) (Figure 2). Solution and refinement in subgroups of *Imma* confirmed that only the pillar carboxylates and water molecules are ordered, there being no long-range correlation in the two orientations of the layers. The cyclohexane ring of the chdc pillar is disordered over two chair-type conformations, each modeled with 50% occupation. The water molecule forms hydrogen bonds with its structurally equivalent neighbors in the channel (O(21)···O(21)′ = 2.952(13) and 2.835(12) Å), with the hydroxyl groups of the layer (O(21)···O(3) = 2.926(11) Å, O(21)···O(3)′ = 2.923(11) Å, O(21)···O(2A) = 3.309(12) Å, O(21)···O(2A)′ = 3.13(11) Å, O(21)···O(2B) = 2.909-(11) Å, O(21)···O(2B)′ = 2.904(11) Å) and with the oxygen atoms of the pillar carboxylate group (O(21)···O(11) = 2.974(7) Å, O(21)···O(12)′ = 3.118(8) Å) (see Table 4).

The optical transmission spectrum for CDCC·4H_2O contains two strong bands at 15700 and 16800 cm^{-1} and a weak

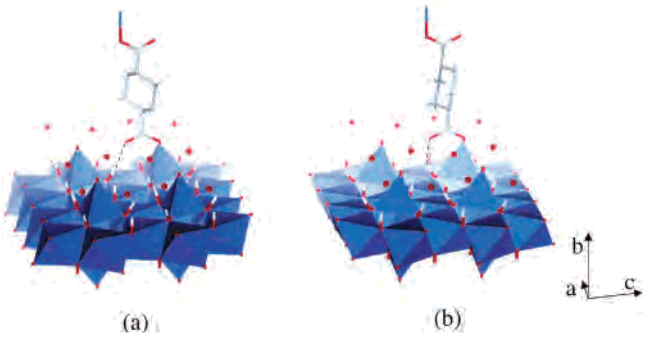

Figure 2. Pillar−layer hydrogen bonding interactions in CDCC·4H_2O, showing the short contacts between the uncoordinated oxygen atom of the pillar carboxylate group to the hydroxyl groups of the 50% disordered layer ((a) layer orientation A; (b) layer orientation B). Hydrogen bonding interactions involving the water molecules, represented as small spheres, are omitted for clarity.

broad band at 20000 cm^{-1}, characteristic of the expected strong $^4A_2 \rightarrow {}^4T_1(P)$ doublet from tetrahedral cobalt and an overlap of the weak $^4T_{1g}(F) \rightarrow {}^4A_{2g}(P)$ and $^4T_{1g}(F) \rightarrow {}^4T_{1g}(P)$ bands from octahedral cobalt, respectively (Figure S4). Due to the large difference in intensity of the $Co(II)^{oct}$ and $Co(II)^{tet}$ bands, the compound has the characteristic blue color of tetrahedral cobalt in a coordination of oxygen atoms. The compound acquires a green tinge, possibly due to changes in surface quality, on dehydration, but there are no noticeable changes in the positions and intensities of the spectral bands.

Reversible Dehydration and Rehydration of the Structure. Thermogravimetric-differential thermal Analysis (TG-DTA) of CDCC·4H_2O in air reveals three weight loss steps in the range 20−1000 °C (Figure S5). The first two and the last are endothermic, and the third is exothermic. The first two, at 80 and 120 °C, each correspond to the loss of two noncoordinated water molecules per formula unit to give the phases CDCC·2H_2O and CDCC, respectively. The third, centered at 200 °C, is the pyrolysis of the chdc pillar to give Co_3O_4 as confirmed by PXRD (JCPDS 1-1152D). The temperatures of each of the dehydration steps depend on the heating rate, indicating a slow equilibration of dehydration process, and on the relative humidity. On cooling the samples rapidly in air, they reversibly reabsorbed atmospheric water to return to their original weights after each of the dehydration steps (Figure 3). The rate of recovery depends on the amount of air, being either slower and without step in a slow stream or fast to the dihydrate followed by a slow uptake to the tetrahydrate in open air. The dehydration/rehydration process was found to remain fully reversible over several cycles of heating and cooling.

Single crystal X-ray diffraction measurements performed in situ with slow heating at 20 °C/h to 102 °C showed that the unit cell remains unchanged up to ca. 40 °C. Above this temperature, the Bragg spots broaden along b^*, the direction perpendicular to the layers. The retention of sharpness along a^* and c^* indicates that the layers retain their full 2-D periodicity and regular stacking with heating. The broadening of the spots along b^* is consistent with a loss of long-range order along the b-axis associated with a variation of interlayer spacing on the short range. In the temperature range 60−80 °C, the diffraction images showed some evidence for an intermediate 13.9 Å phase, as observed in the PXRD measurements (see the following description), although the extreme streaking of the diffraction spots in this range prevented a useful analysis. With further heating to 102 °C, the crystal was fully dehydrated to CDCC, as confirmed by comparison with the PXRD results. At this temperature, the streaking along b^* decreased, indicating a conversion of all domains within the crystal to CDCC and an increased long-range ordering of the interlayer spacing with full dehydration. The unit cell of CDCC is approximately halved along both the a- and b-directions. The symmetry reduces from body-centered orthorhombic *Imma* to triclinic $P\bar{1}$, with α and γ decreasing from 90° to 85.460(11)° and 82.686(11)°, respectively, and β, which lies in the plane of the layer, remaining approximately unchanged at 89.954(9)°.

The principal change to the structure on removal of the water molecules is a slippage of the layers with a tilting and rotation of the chdc pillars (Figure 4) and a concomitant shortening of the interlayer separation from 14.5 to 13.4 Å. A similar layer slippage has been proposed in other porous metal−organic hybrid materials.[23,39] There is an accompanying volume contraction of 35.1(2) $Å^3$ per formula unit, equivalent to 8.8 $Å^3$ per water molecule lost from the structure. This comparatively small volume contraction is reflected in a decrease in the calculated density of the material from 2.283 to 2.202 g cm^{-3}, indicating a less efficient crystal packing. Despite this, CDCC has a zero calculated void volume (i.e., no region of the structure lies more than 1.2 Å away from the van der Waals surface of the framework),[38] the 1-D channels in CDCC·4H_2O having disappeared with the tilting and rotation of the pillars (Figure 5). There are no appreciable changes to the Co−O bond lengths and angles with dehydration to CDCC (see Tables 2 and 3), the mean tetrahedral and octahedral Co−O distances at 102 °C being 1.94(3) and 2.12(3) Å. The approximate halving of the unit cell along the b-axis results from a loss of the $c/2$ translation (2.70 Å along the c-direction) of neighboring layers in the body-centered orthorhombic cell to a translation of $0.76a + 0.22c$ (i.e., 4.72 Å in the a-direction and 1.21 Å in the c-direction) to give a triclinic cell. The increased tilting of the chdc pillars corresponds to an increase in the total translation between neighboring layers from 2.70 to 4.86 Å. In contrast to the parent material, which has only one apparent orientation of the chdc carboxylate group despite two separate hydrogen bonding arrangements to the disordered layer (Figure 2), the dehydrated material has two observed carboxylate orientations, each with 50% occupation (Figure 6). The disorder arises with the tilting of the pillar and the rotation of the carboxylate into one of two orientations depending on hydrogen bonding interactions with the 2-fold disordered layer. The carboxylate groups for each orientation rotate to a differing degree, one rotating by 49° to form two new hydrogen bonds to the A orientation of the layer with distances O(1A)···O(12A) = 2.61(18) Å and

(39) Kitagawa, S.; Kitaura, R. *Comments Inorg. Chem.* **2002**, *23*, 101. Biradha, K.; Hongo, Y.; Fujita, M. *Angew. Chem., Int. Ed.* **2002**, *41*, 3395.

Table 4. Hydrogen Bond Analysis for CDCC·4H_2O, CDCC, and Rehydrated CDCC·4H_2O[a]

		CDCC·4(H_2O)				CDCC	
		virgin (−123 °C)	rehydrated (22°C)	rehydrated (−123°C)		(102 °C)	(−123 °C)
		Donor···Acceptor					
pillar−layer	O1A···O12	2.797(17)	2.76(2)	2.77(2)	O1A···O12A	2.61(18)	2.02(9)
	O1B···O12	2.707(16)	2.63(2)	2.64(2)	O3A···O12A	3.3(2)	3.14(11)
					O2B···O12B	2.88(16)	2.88(8)
guest−layer	O21···O2A	3.309(12)	3.332(17)	3.307(15)			
	O21···O2B	2.909(11)	2.902(16)	2.927(15)			
	O21···O3	2.926(11)	2.931(16)	2.928(15)			
	O21···O2B_3	2.904(11)	2.904(16)	2.911(14)			
	O21···O3_2	2.923(11)	2.930(16)	2.910(15)			
	O21···O2A_4	3.313(11)	3.330(17)	3.287(15)			
guest−pillar	O21···O11	2.974(7)	2.979(10)	2.965(8)			
	O21···O12_1	3.118(8)	3.132(12)	3.117(11)			
guest−guest	O21···O21_6	2.835(12)	2.838(19)	2.813(17)			
	O21···O21_5	2.952(13)	2.942(20)	2.928(18)			

[a] Operators for generating equivalent atoms: 1, $x, y, z + 1$; 2, $-x + 1, -y + {}^3/_2, z - 1$; 3, $-x + {}^1/_2, y, -z + {}^3/_2$; 4, $-x + 1, -y + 2, -z - 1$; 5, $-x + {}^3/_2, y, -z - {}^1/_2$; 6, $-x + {}^3/_2, y, -z + {}^1/_2$.

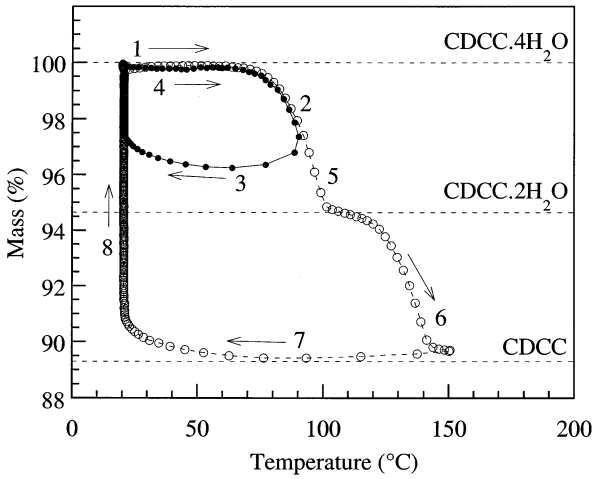

Figure 3. Thermogravimetry of CDCC·4H_2O in air. The material undergoes a two-step dehydration, converting to CDCC·2H_2O at 100 °C and to CDCC at 150 °C with heating at 30 °C/h. Cooling of the partially and fully dehydrated phases in air leads to rapid rehydration to return to the original mass. The numbers 1−8 indicate the progression of a cyclic desorption/sorption experiment on a single sample.

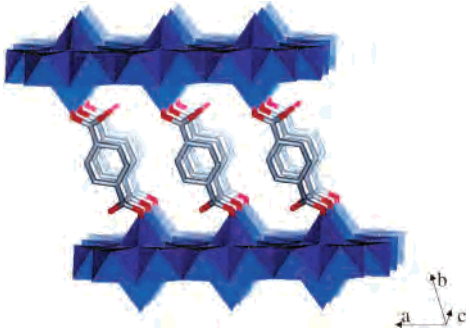

Figure 4. Polyhedral representation of the crystal structure of CDCC, which contains tilted chdc pillars. Hydrogen atoms, and the 50% layer and pillar disorder, are omitted for clarity.

O(3A)···O(12A) = 3.3(2) Å (Figure 6a, Table 4) and the other rotating by 60° to form one new hydrogen bond to the B orientation of the layer with a distance O(2B)···O(12B) = 2.88(16) Å (Figure 6b, Table 4). A long-range alternating alignment of the carboxylate pillars lying at $x \sim 0$ and $x \sim {}^1/_2$ in the hydrated phase is lost through the transition, leading to a halving of the *a*-parameter.

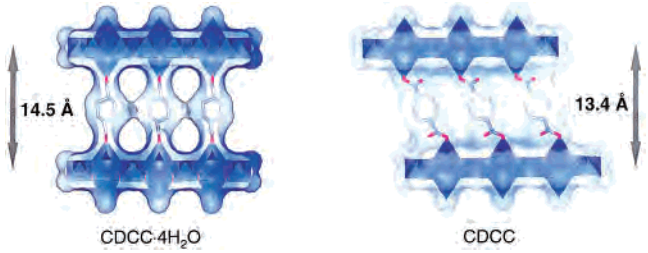

Figure 5. Pore surface diagrams of (a) CDCC·4H_2O, which contains 13.4% pore volume occupied by water, and (b) CDCC, which has zero pore volume due to the tilting of the pillars and decrease in the interlayer separation.

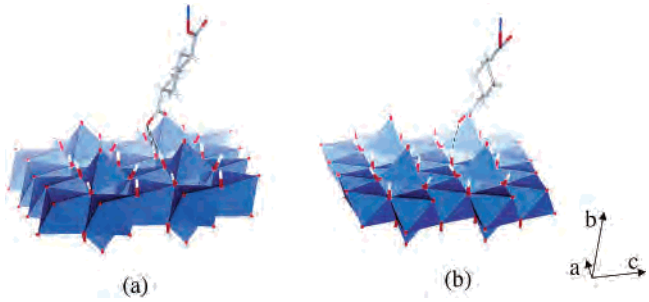

Figure 6. Pillar−layer hydrogen bonding interactions in CDCC ((a) layer orientation A; (b) layer orientation B).

Rehydration of the crystal to CDCC·4H_2O on exposure to air led to a sharpening of the diffraction pattern, although the streaking of spots along the *b**-direction remained to some extent (Figure S1). Structural refinements at 22(2) and −123(2) °C indicate that the material was returned to its original form. The unit cell dimensions of the virgin and rehydrated structures at −123(2) °C are closely similar although they lie outside of the estimated errors. This discrepancy that may be due to systematic errors in the indexing caused by the spot broadening for the rehydrated crystal and to an underestimation of the cell errors. A close comparison of the structural refinements of the virgin and rehydrated crystal at −123(2) °C reveals that the atomic positional and thermal parameters are the same within error, the average relative atomic shift being 0.02 Å (average shift/error = 0.54) and the average absolute shift/error for the thermal parameters being 0.81 (see Table S1 of the Supplementary Information). The close similarity of the thermal

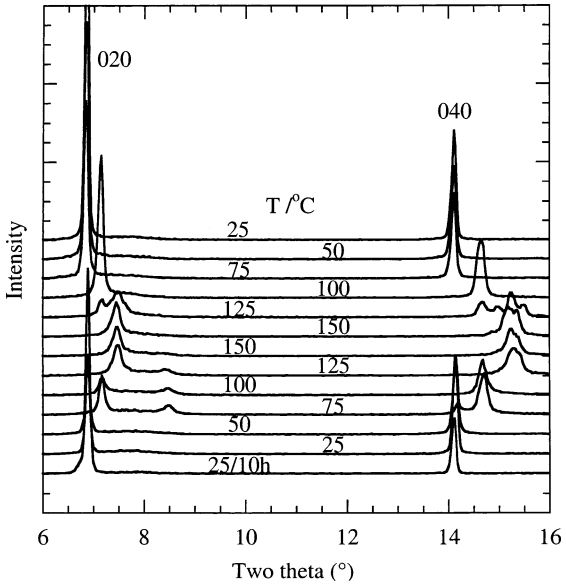

Figure 7. Temperature-dependent powder X-ray diffraction patterns, showing full reversibility of the dehydration/rehydration of CDCC·$4H_2O$. The patterns were recorded with heating from 25 °C (top pattern) to 150 °C and then cooling in air to 25 °C. Patterns in the temperature ranges 20−50, ca. 75−100, and 125−150 °C correspond primarily to the phases CDCC·$4H_2O$, CDCC·$2H_2O$, and CDCC, respectively.

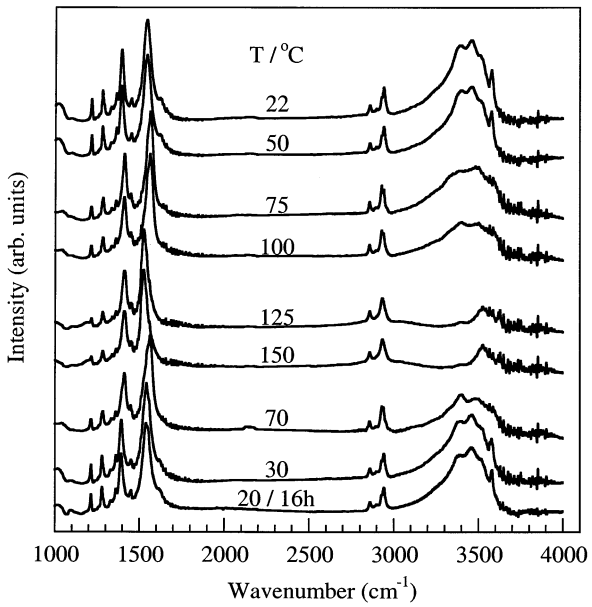

Figure 8. Temperature-dependent infrared spectra showing full reversibility in the dehydration/rehydration of CDCC·$4H_2O$. The spectra were recorded with heating from 22 °C (top spectrum) to 150 °C and then cooling in air to 20 °C (bottom spectrum). Spectra in the temperature ranges 20−50, ca. 70−100, and 125−150 °C correspond to the phases CDCC·$4H_2O$, CDCC·$2H_2O$, and CDCC, respectively.

parameters of the solvent water molecule is consistent with full rehydration of the structure.

Ex-situ PXRD investigations of the thermal dehydration/rehydration chemistry in air indicated that the partially and fully dehydrated phases CDCC·xH_2O ($0 \leq x < 4$) rapidly absorb atmospheric water to return to the fully hydrated phase. Subsequent in-situ investigations were performed both with heating/cooling in air and in vacuo on the INEL instrument. Samples heated to 100 °C showed a shift in the 0*k*0 peaks corresponding to a decrease in the interlayer spacing from 14.5 to 13.9 Å (Figure 7). With heating to 150 °C, a further decrease in the interlayer spacing to 13.3 Å was observed at 125 °C. These observations are consistent with the TG-DTA findings of a first step dehydration from virgin CDCC·$4H_2O$ to CDCC·$2H_2O$ followed by a second step to the anhydrous phase, CDCC. The diffraction peaks broaden reversibly with dehydration, the fwhm of the interlayer peak (020 for CDCC·$4H_2O$ and 010 for CDCC·$2H_2O$ and CDCC) increasing from 0.08° (approximately equal to the instrument dispersion) to 0.14° to 0.18° (Figure 7). This behavior is consistent with the observed broadening of the SCXRD spots and is attributed to a decrease in correlation length of the interlayer spacing upon dehydration. With rehydration in air, the reverse process is observed, and the diffraction peaks sharpen considerably, indicating an increased long-range ordering of the interlayer spacing. For rehydrated CDCC·$4H_2O$, the interlayer peak 020 is slightly broader (fwhm = 0.12°) than that of the virgin material, indicating a slight decrease of structural order following dehydration/rehydration. This may reflect either a small degree of pillar disorder, as suggested by the SCXRD results, or an incomplete rehydration of the sample. Investigations of the dehydration chemistry were also made in situ under dynamic vacuum at 16 °C. At a pressure of 10^{-1} Torr, the PXRD pattern remained essentially unchanged from that of the virgin sample over a period of 1 h. On decreasing the pressure to 5×10^{-5} Torr at 16 °C, the 0*k*0 peaks split first into two and then into three, corresponding to the gradual formation of the 13.9 Å CDCC·$2H_2O$ and then 13.3 Å CDCC phases. The anhydrous form appears to be indefinitely stable in a vacuum. On purging with air, the process is reversed over a period of 2 h, the anhydrous CDCC returning to CDCC·$4H_2O$ via the CDCC·$2H_2O$ intermediate (Figure S6).

Investigation of the crystal quality by scanning electron microscopy and electron diffraction revealed that virgin samples dehydrated by evacuation within the SEM instrument did not show any obvious crystal damage (Figure S7a). A sample that had previously been heated rapidly to 150 °C in the TG-DTA, however, showed cracks and splitting of the crystallites, indicative of a degree of crystal strain caused by an inhomogeneous distribution of crystallite water during the structural transition (Figure S7b). Diffraction patterns taken normal to the crystallite platelets showed the expected 5.4×6.2 Å^2 periodicity, confirming the presence of the $Co^{(oct)}{}_3Co^{(tet)}{}_2(OH)_8$ layer (Figure S8).[27]

The temperature-dependent infrared spectrum, recorded in-situ with heating and cooling in air, is shown in Figure 8. Several bands were observed, and we assign here only the regions of the spectrum that vary appreciably with temperature. Of the hydroxyl stretching modes in the region 3300−3600 cm^{-1}, those at higher energy appear sharper and are assigned to the hydroxyl groups, and those at lower energy, which are broader, are assigned to the water of crystallization. On warming to 100 °C to give CDCC·$2H_2O$, the intensities of the two water bands decreased to approximately half that of the virgin sample. With further heating to 125 °C to give CDCC, these bands disappeared completely leaving a broad hydroxyl band at 3525 cm^{-1}. The bending mode of H_2O at

1650 cm^{-1} showed a similar behavior with heating. On cooling overnight in air, all of the water bands reappeared, and the spectrum was returned to that of the virgin sample. A second set of bands between 2800 and 3000 cm^{-1} are assigned to the stretching modes of the methylene groups. Only a slight, reversible change is observed for these bands with heating and cooling. In a third set of bands, peaks at 1540 and 1400 cm^{-1} are assigned, respectively, as the antisymmetric and symmetric stretching modes of the carboxylate groups. The absolute energies and difference in energy (Δ) of these two bands are sensitive to the mode of coordination of the carboxylate group and are therefore useful in assigning the modes of coordination.[40] We have previously characterized three different modes of coordination, a unidentate, a bis-unidentate, and a tris-unidentate in related materials.[30] The antisymmetric band moves reversibly from 1540 cm^{-1} for CDCC·$4H_2O$ to 1560 cm^{-1} for CDCC·$2H_2O$ to 1524 cm^{-1} for CDCC. Correspondingly, the symmetric band shifts reversibly from 1392 cm^{-1} for CDCC·$4H_2O$ to 1410 cm^{-1} for CDCC·$2H_2O$ and CDCC. The shifting of these bands reflects the competition of hydrogen bonding of the carboxylate group with the water of crystallization and the hydroxyl groups of the framework. The importance of hydrogen bonding is manifested by a change in Δ, the difference between the energies of the two bands, viz. 148 cm^{-1} for CDCC·$4H_2O$, 150 cm^{-1} for CDCC·$2H_2O$, and 114 cm^{-1} for CDCC. The O−C−O bending modes at 778 and 630 cm^{-1} also appear to be sensitive to the presence of water molecules, although band overlap in this region prevented a useful analysis. The bands belonging to the cyclohexane backbone are unaltered by the dehydration process.

Magnetic Properties. The temperature-dependent magnetic susceptibility of polycrystalline samples of CDCC·$4H_2O$ in an applied field of 25 Oe is shown in Figure 9. The data were taken on cooling the sample in a helium flow first from 300 to 2 K and then warming to 275 K and stabilizing for 30 min, followed by data collecting to 400 K. The PXRD measurements performed in vacuo indicate that the brief evacuation of the polycrystalline sample in the magnetometer at 125 K prior to measurement would be insufficient to cause any appreciable dehydration of the sample. The sample was kept at 400 K for 1 h to fully dehydrate it to CDCC before taking data on cooling to 2 K. A second sample was measured after it had been heat-treated to 150 °C for 1 h and exposed to air for 3 weeks to fully rehydrate the sample. The data for all three materials were nearly identical, indicating that the magnetic properties are highly insensitive both to the extent of hydration and to the dehydration/rehydration history of the sample. The data above 150 K obey the Curie−Weiss law with a Curie constant of 12.5(4) cm^3 K/mol and a Weiss constant of −67(8) K. The effective moment of 4.5 μ_B per cobalt is the expected average for tetrahedral and octahedral cobalt(II) ions with the $Co^{(oct)}_3$-$Co^{(tet)}_2$ stoichiometry. With cooling, the moment decreases gradually to a minimum at 120 K before increasing rapidly at low temperatures. The observation of a shallow minimum in the moment is as expected for a ferrimagnet. The maximum value of χT is dependent on the applied field, being larger in a small field due to the nonlinear variation of the magnetization with field as the transition temperature (60.5 K) is approached and to moment saturation below this temperature.

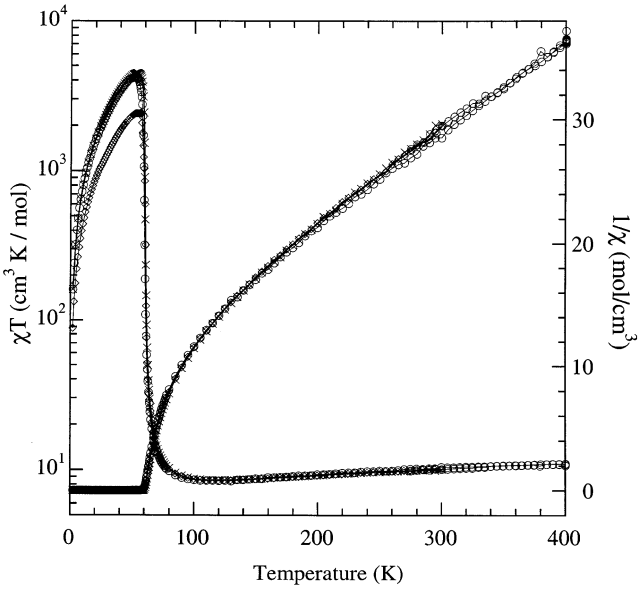

Figure 9. Temperature dependence of the inverse magnetic susceptibility and of the product of susceptibility and temperature: virgin CDCC·$4H_2O$ (○), CDCC (×), and rehydrated CDCC·$4H_2O$ (◇).

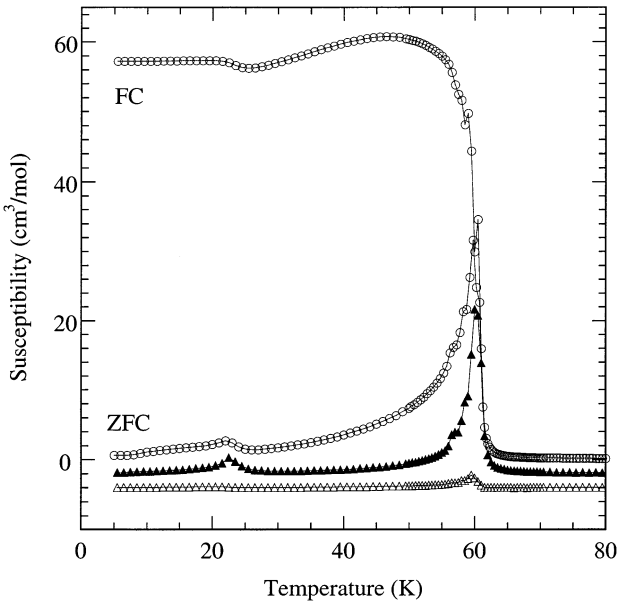

Figure 10. Temperature dependence of the magnetic susceptibilities in a dc and ac field of 1 Oe: χ_{dc} (○, ZFC and FC), χ' (▲), χ'' (△). [Note that the real and imaginary ac susceptibilities are offset by −2 and −4 cm^3/mol, respectively.]

Data obtained on a virgin polycrystalline sample in an applied dc magnetic field of 1 Oe after zero-field-cooling (ZFC) and field-cooling (FC) in the same field are shown in Figure 10. A very clear and sharp bifurcation point is evident at 60.5 K, and long-range ferrimagnetic ordering with spontaneous magnetization is observed below this temperature. The magnetization in the ordered state is lowered

(40) Deacon, G. B.; Phillips, R. J. *Coord. Chem. Rev.* **1980**, *33*, 227. Nakamoto, K. *Infrared and Raman Spectra of Inorganic and Coordination Compounds*, 5th ed.; John Wiley and Sons: New York, 1997.

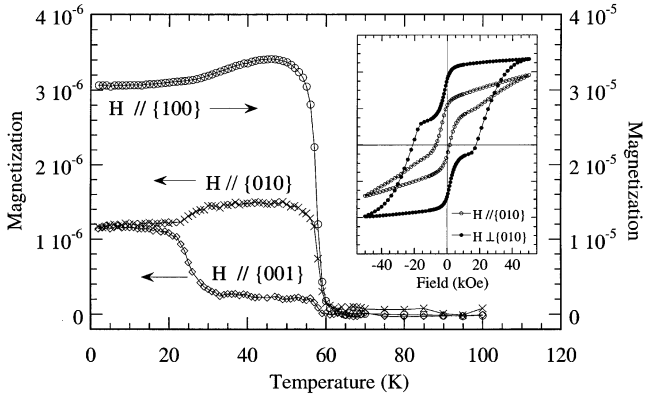

Figure 11. Temperature-dependent magnetization of CDCC·$4H_2O$ along each of the crystallographic axes, measured in a field of 100 Oe on an aligned single crystal. Due to the very small mass of the crystal, we are unable to give absolute values of the magnetization. Units are therefore arbitrary although they were scaled consistently between the three measurements. The inset shows the orientation dependence of the magnetization at 2 K, measured on an array of aligned crystals.

below 50 K, suggesting either that the anisotropic field is stronger than the applied field thus creating a multidomain structure even in a small applied field, or that there exist two magnetic sublattices having different temperature-dependent magnetizations to give a P-type Néel antiferromagnet.[41,42] The P-type appears when the sublattice with smaller moment is thermally disturbed more easily. The ferrimagnetic transition is accompanied by sharp peaks in the real and imaginary components of the ac susceptibilities measured in a field of 1 Oe oscillating at 20 Hz. The sharpness of the ac susceptibility peaks characterizes this compound as a hard magnet, the large magneto-crystalline anisotropy resulting in large coercive fields.

The data collected in small applied fields display an anomaly at 23 K in the form of kinks in both the dc and ac susceptibilities (Figure 10). This feature is present in other compounds that contain the $Co^{(oct)}{}_3Co^{(tet)}{}_2(OH)_8$ layer[27] and has been interpreted previously as being due to a contribution from an impurity phase related to $Zn_5(OH)_8Cl_2·H_2O$.[43] This possibility is unlikely here given there is no evidence for impurities in the PXRD and SEM measurements. To verify if the transition at 23 K is intrinsic to the material, the magnetization of a single crystal was measured on cooling in a field of 100 Oe (Figure 11). Significantly, both transitions were observed, and their dependence on the orientation of the crystal is quite pronounced. The magnetization along the *a*-axis is ca. 20 times that along the two orthogonal axes, indicating that the easy axis lies in the plane of the crystal with a major magnetization component along the *a*-axis. The transition at 23 K is manifested by a gain in magnetization along the *c*-component and a loss along the *a*- and *b*-components. Such changes may, therefore, be associated with a reorientation of the magnetization within the plane of the layers.

The isothermal magnetization was measured on an array of oriented crystals at 2 K (Figure 11) and on powder samples as a function of temperature from above the Curie temperature to 2 K. The data taken on a polycrystalline sample on the VSM up to 1.8 kOe are shown in Figure S9. The isothermal magnetization is linear with field for temperatures above 68 K but exhibits unusual behavior near the Curie temperature. At 64 K, the magnetization starts to exhibit a small curvature that fits the Langevin function. At 63 K, the curvature is slightly more pronounced, and in addition, a small remanent magnetization is observed. As the temperature is lowered to 50 K, the remanent magnetization increases until it attains a square shape with negligible coercivity. The data can be approximately fitted as a sum of a Langevin function and a hysteresis loop with zero coercivity. The parameters obtained from this fit suggest (a) superparamagnetism just above the Curie temperature with an increase of coherence length as the temperature is lowered, and (b) an increase in hysteretic behavior due to blocking as the coherence length increases on lowering of the temperature. The coercivity increases gradually with cooling to 25 K. Below this temperature, the shape of the hysteresis becomes more rounded and the coercive field increases more rapidly until it attains a value of 22 kOe at 2 K. These changes coincide with the transition at 23 K and appear therefore to result from the reorientation of the moment within the layers. The hysteresis curves for an array of aligned crystals at 2 K are given in the inset of Figure 11. When the field is parallel to the layers, the curve exhibits a superposition of two loops, one with a small coercive field and the other with a large one. The magnetization attains saturation at high field. For the applied field perpendicular to the layers, the hysteresis is narrow, and the magnetization does not attain saturation. These observations are consistent with the easy axis lying parallel to the layers.

The reduction of the magnetization at lower temperature is possibly due to the large magnetic hardness of these compounds. The material exhibits a pronounced temperature dependence of its coercive fields that attain 22 kOe at 2 K. We note that the 50 kOe maximum field of our SQUID magnetometer is not sufficient to fully reverse all of the moments for the powder sample.

Discussion

We have recently reported other pillared phases, $M^{(oct)}{}_3M^{(tet)}{}_2(OH)_8$, layer where a lack of 3-D ordering was attributed to an aperiodic slippage of adjacent layers and to an absence of through-layer communication of the interlayer geometry to cause twinning over the short range.[27] In such cases, only the interlayer spacing may be derived from diffraction data. The achievement of 3-D crystallographic ordering here has been achieved uniquely for this layer type through the use of the chdc pillar, which confers a periodic slippage (*c*/2 translation) of adjacent layers. The structural ordering achieved in CDCC·$4H_2O$ contrasts with that of the diamine-pillared Namuwite-type layer ($M^{(oct)}{}_3M^{(tet)}(OH)_6(SO_4)$) materials, in which the tetrahedral metal sites from neighboring layers are eclipsed due to perpendicular pillaring by 1,2-diaminoethane (AAA-stacked) and 1,4-diazabicyclo[2,2,2]-octane (ABA-stacked).[26]

(41) Herpin, A. *Theorie du Magnetisme*; Presse Universitaire de France: Paris, 1968.
(42) Néel, L. *Ann. Phys.* **1948**, *3*, 137.
(43) Allmann, R. *Z. Kristallogr.* **1968**, *126*, 417.

The full ordering of the pillar carboxy groups within CDCC·$4H_2O$ is highly unusual given the 50% disorder of the layers. This feature may be attributed to the ability of the chdc pillar to bind with equal geometry to each of the two orientations of the disordered layer and to an intralayer communication of carboxylate orientation through a subtle distortion of the layer. The layer distortion is most pronounced for the hydroxyl groups that hydrogen bond to the pillar carboxylates (atoms O1A and O1B lie 1.271 and 1.108 Å from the mean plane of the layer; see Figure S10). This distortion directs the carboxylate groups on either side of the layer to have opposite effective orientations. As a result, the pillars are oriented uniformly within the structure, albeit with disorder of the cyclohexane ring, while each inorganic layer to which they are hydrogen bonded is randomly disordered in one of two orientations. Similarly, within the resolution of the SCXRD data, the solvent water molecule occupies a single site within the 1-D channel, as located by hydrogen bonding interactions to neighboring water in the channels, to the pillar carboxylate groups and to the disordered hydroxyl groups of the layer.

Characterization of the thermal dehydration of CDCC·$4H_2O$ by single crystal and powder X-ray diffraction, thermogravimetry, and vibrational spectroscopy indicates that water loss is a fully reversible process. The structural flexibility of the chdc pillars and their mode of hydrogen bonding to the layer allows the structure to relax to a dense configuration with removal of the water molecules. The 1-D channels of the hydrated material disappear through the CDCC·$4H_2O \rightarrow$ CDCC transition with a tilting and rotation of the pillars and the decrease in the interlayer spacing from 14.5 to 13.3 Å. A similar structural transformation was observed for $Co_4(SO_4)(OH)_6(en)_{0.5}\cdot 3H_2O$ (en = 1,2-diaminoethane),[26] where there is a one-step water removal and corresponding decrease in the interlayer spacing from 10.5 to 9.3 Å. In that case, 3-D ordering was lost in the transformation, apparently due to an insufficient steric communication of pillar orientation through the layers. In contrast, the CDCC·$4H_2O \leftrightarrow$ CDCC transition occurs with retention of 3-D structural ordering, a remarkable feature that has allowed single crystal structural characterizations of both the dehydrated and rehydrated phases. We note here that orthorhombic to triclinic transitions are commonly expected to lead to 4-fold crystallographic twinning, resulting in planes of diffuse scattering parallel to the a^*c^*-plane if occurring on the short range or four separate reciprocal lattices if occurring within separate crystal domains. For CDCC, the sharpness of the spots in the a^*c^*-plane indicates a long-range ordering of the unit cell tilting. Further, the diffraction pattern could be indexed using a single triclinic cell to leave only a small number of weak spots corresponding to a misaligned twin with a twinning fraction of ca. 10%. This indicates that the majority of the crystal tilted in the same direction with the orthorhombic to triclinic transition, a conclusion that is consistent with the observation of angled side faces in SEM images of CDCC crystal platelets (Figure S7) as compared to the perpendicular {1,0,0}, {0,1,0}, and {0,0,1} faces of the orthorhombic CDCC·$4H_2O$. The presumed mechanism for the long-range cooperative tilting of the unit cell is a steric communication of the pillar geometry through a local distortion in the layer, similar to that responsible for the pillar ordering in CDCC·$4H_2O$. Verification of this mechanism through accurate analysis of the pillar-layer geometry in CDCC was not possible due to the low quality diffraction data and the 50% carboxylate-layer disorder. Further, the extreme disorder of the pillars and low data quality leads to some ambiguity of the overall pillar orientation in CDCC. We note here that the structural transition as modeled necessitates a detachment and recoordination of half of the pillar carboxylate groups, as may be facilitated via exchange of this group with the solvent water molecules. However, the diffraction and IR data are inconclusive on this point, and further characterizations, including examination of the partially dehydrated phase CDCC·$2H_2O$, are planned to investigate the structural mechanism of the dehydration transition.

Characterizations of the dehydration/rehydration chemistry by powder X-ray diffraction and vibrational spectroscopy are consistent with the single crystal X-ray analyses. With dehydration, the infrared spectra display a characteristic loss of water bands, and there is strong evidence for a change in the mode of hydrogen bonding for the carboxylate groups of the pillar. The data do not allow a definitive assignment of the mode of carboxylate binding in CDCC·$2H_2O$. The observation of a separate band for CDCC·$2H_2O$ confirms that this is a distinct structural phase rather than a structural "average" of the fully hydrated and dehydrated phases. The observation of discontinuous changes to the powder X-ray diffraction pattern and broad backgrounds between the *0k*0 peaks with the CDCC·$4H_2O$ (14.5 Å) $\leftrightarrow$ CDCC·$2H_2O$ (13.9 Å) $\leftrightarrow$ CDCC (13.3 Å) dehydration/rehydration steps, rather than a continuous shift of a distinct interlayer spacing, indicates a loss of crystallographic long-range order for the partially hydrated intermediate phases. These observations correspond to the extreme spot-streaking seen in the single crystal measurement with partial dehydration at intermediate temperatures. To our knowledge, such a loss then regain of 3-D monocrystallinity is novel for molecular hybrid systems.

One of the key questions regarding the long-range magnetic ordering in layered systems is that of the magnetic dimensionality. Here, the presence of superparamagnetism above the Curie temperature, as evidenced by the nonzero imaginary component in the ac susceptibilities and the weak remanence, suggests strong correlation within the layer. The magnetic dimensionality may therefore be considered as 2-D above the transition. With cooling to the transition temperature, the number of correlated sites increases, giving clusters of large moments. At the transition, the small through-space (dipolar) coupling results in the 3-D long-range ordering of the moments. The magnitude of the dipolar field depends on the orientation of the moments within the layer; it is expected to be small if the moments are aligned perpendicular to the layer and large when parallel.[44] Therefore, long-range magnetic ordering can take place at fairly large distance for

(44) De'Bell, K.; Maclsaac, A. B.; Whitehead, J. P. *Rev. Mod. Phys.* **2000**, *72*, 225.

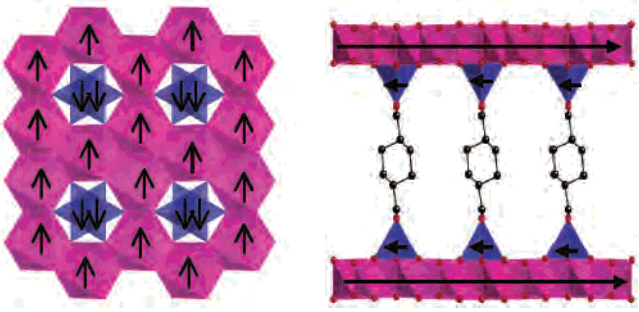

Figure 12. Diagrammatic representation of the proposed magnetic ordering at the tetrahedral and octahedral cobalt(II) sites within the $Co^{(oct)}{}_3Co^{(tet)}{}_2(OH)_8$ layer.

the latter orientation of the moments. Furthermore, for this mechanism the Curie temperature is expected to be very weakly dependent on the distance or the chemical nature of the content between the layers, which is consistent both with the lack of any appreciable change to the magnetic properties of CDCC·$4H_2O$ upon dehydration and with the previous observations of similar Curie temperatures for other materials containing the $Co^{(oct)}{}_3Co^{(tet)}{}_2(OH)_8$ layer.[27] The single crystal magnetic measurements clearly indicate that the moments lie in the plane of the layer, thereby favoring the dipolar coupling. The large observed anisotropy is consistent with either a 2-D Ising or an XY type magnet.[11] The large coercive field for materials of this layer type was previously interpreted as being due to a perpendicular alignment of the moment assuming a Heisenberg system;[27] however, the present isothermal magnetization data demonstrate that the moments are in fact in the plane of the layer with the easy axis along the *a*-axis. The large magnetocrystalline anisotropy is a contribution of several components, such as (a) the large single-ion contribution due to the stabilization of an effective $s = {}^1/_2$ and large and anisotropic *g*-values[45] of the divalent cobalt, (b) the large shape anisotropy of the crystals, and (c) the dipolar field.[46]

The value of the saturation magnetization of 2 μ_B is consistent with a two-sublattice ferrimagnet where one comprises the three octahedral cobalt atoms, and the other the two tetrahedral cobalt atoms (Figure 12). Given that the spin−orbit coupling is higher for octahedral cobalt than for tetrahedral cobalt, and that the magnetization is, respectively, lower, the resultant magnetization of three octahedral cobalt aligning antiparallel to the two tetrahedral cobalt is found to be 2 μ_B per formula unit instead of 3 μ_B if the spin quantum numbers were applicable.

The occurrence of pretransitional magnetic ordering, as evidenced by the observation of remanent magnetization and nonlinear ac susceptibilities, is highly unusual. This may be a consequence of the high crystallinity of the sample in the present case. Such pretransitional short range orderings would normally be obscured by particle-size effects and impurities. Fitting of the low field (1 Oe) field-cooled magnetization data of a powdered sample in the temperature range 55−65 K to the exponent function, $M = M_s(T_C - T)^{\beta}$,[47] gave T_C = 61.05(4) K and β = 0.25(3). The critical exponent is consistent with that expected for XY magnets.[48]

There are several other features of the magnetic properties worthy of comment. The transition is much sharper than those reported for less crystalline cobalt(II)−hydroxide analogues.[27] We note also that the bifurcation takes place nearly at the midpoint of the FC data, in contrast to that expected for 3-D compounds.[49] The sharp peaks in the ac susceptibilities and the coincident maxima of the real and imaginary components are characteristic of a 2-D material, as seen also in analogous 2-D compounds.[27] In contrast, 3-D compounds typically have a temperature at which the nonzero imaginary susceptibility coincides with that of the peak in the real component. An important question arises here on the definition of the Curie temperature; in general, this is defined as the temperature of the maximum of the ac real susceptibility or the nonzero value of the imaginary part, or at the bifurcation point in a very low-field ZFC−FC dc magnetization.[41] Here, we define it by the first and last criteria, each of which give a value of 60.5 K. The roundness in the magnetization curve before the transition and the nonzero imaginary component suggests an exponential increase of the correlation length within the layer before the entire compound orders magnetically.

Conclusions

The present work provides a structural and physical characterization of a pillared layer material that shows long-range magnetic ordering and guest-exchange properties. The successful synthesis of single crystals, which is rare for pillared layer materials and has been achieved here fortuitously through the use of a pillar that confers a periodic slippage of neighboring layers, has allowed a full structural determination of this material. Further, a remarkable retention of 3-D structural ordering with reversible dehydration and rehydration has allowed a detailed investigation of the guest-dependent structure. Of particular structural interest is the observed change in the mode of pillar−layer binding and accompanying decrease in the interlayer spacing with dehydration. To our knowledge, such a structural investigation is unique for a pillared layer material having flexible pillars.

The material orders as a ferrimagnet at 60.5 K, a temperature that is among the highest seen for spontaneous magnetization in an ordered crystalline inorganic−organic hybrid material. Further, the observation of reversible guest-exchange in a magnetically ordered material is novel and has provided the opportunity to study the effect of guest-exchange on magnetic properties. It is of interest, given the expected importance of the through-space interlayer magnetic coupling to the 3-D ferrimagnetic ground state, that the magnetic properties are highly insensitive to the considerable structural perturbation that arises with dehydration. Further work in this area, including variation of the dicarboxylate

(45) Abragam, A.; Bleaney, B. *Electron Paramagnetic Resonance of Transition Ions (International Series of Monographs on Physics)*; Clarendon Press: Oxford, 1970.
(46) Chikazumi, S. *Physics of Ferromagnetism*; Oxford University Press: Oxford, 1992. Bertotti, G. *Hysteresis in Magnetism*; Academic Press: London, 1998.
(47) Stanley, H. E. *Introduction to Phase Transitions and Critical Phenomena*; Clarendon Press: Oxford, 1991.
(48) Bramwell, S. T.; Holdsworth, P. C. W. *Phys. Rev. B* **1994**, *49*, 8811.
(49) Kurmoo, M.; Kepert, C. J. *New J. Chem.* **1998**, *22*, 1515.

pillar and inclusion of magnetic guests (including possible magneto-selective guest exchange), would be of interest.

Acknowledgment. This work was supported by the CNRS-France, the Australian Research Council, and the Royal Society of Chemistry, U,K. H.K. thanks the JSPS-Japan for a young scientist fellowship for his one-year stay in Strasbourg. We are grateful to Drs. M. Richard-Plouet and N. Viart for the electron microscopy work and to Prof. K. Inoue for fruitful discussions.

Supporting Information Available: Experimental details, including UV−vis spectral data, DT-TGA, PXRD, electron microscopy, isothermal magnetizations at different temperatures, and full X-ray structure refinement details (including ORTEP diagrams, crystal data and structural refinements, tables of coordinates, bond lengths, bond angles, anisotropic refinement parameters, and hydrogen bond geometries). This material is available free of charge via the Internet at http://pubs.acs.org.

IC034787G